

We are IntechOpen, the world's leading publisher of Open Access books Built by scientists, for scientists

6,900

Open access books available

186,000

International authors and editors

200M

Downloads

Our authors are among the

154

Countries delivered to

TOP 1%

most cited scientists

12.2%

Contributors from top 500 universities



WEB OF SCIENCE™

Selection of our books indexed in the Book Citation Index
in Web of Science™ Core Collection (BKCI)

Interested in publishing with us?
Contact book.department@intechopen.com

Numbers displayed above are based on latest data collected.
For more information visit www.intechopen.com



Avalanche Photodiodes in High-Speed Receiver Systems

Daniel S. G. Ong and James E. Green
*University of Sheffield
United Kingdom*

1. Introduction

The avalanche photodiode (APD) is widely used in optical fibre communications (Campbell, 2007) due to its ability to achieve high internal gain at relatively high speeds and low excess noise (Wei et al., 2002), thus improving the system signal-to-noise ratio. Its internal mechanism of gain or avalanche multiplication is a result of successive impact ionisation events. In an optical receiver system, the advantage of internal gain, in the APD, is experienced when the amplifier noise dominates that of a unity-gain photodiode. This increases the signal-to-noise ratio (SNR) and ultimately improves the receiver sensitivity as the gain increases until the APD noise rises to become dominant.

Indium Phosphide (InP) is widely used as the multiplication layer material in commercially available APDs for applications in the 0.9–1.7 μm wavelength region with $\text{In}_{0.53}\text{Ga}_{0.47}\text{As}$ grown lattice-matched to it as the absorption layer. It has been predicted that Indium Aluminium Arsenide ($\text{In}_{0.52}\text{Al}_{0.48}\text{As}$) will replace InP, as a more favourable multiplication layer material due to its lower excess noise characteristics (Kinsey et al., 2000). In comparison to InP, tunnelling currents remain lower in InAlAs due to its larger bandgap. While holes ionise more readily than electrons in InP, the opposite holds true for InAlAs and InGaAs, as electrons ionise more readily than holes; thus making the InGaAs/InAlAs combination superior to InGaAs/InP in a SAM APD, in terms of lower excess noise, higher gain-bandwidth product, and improved sensitivity. Studies have also shown that the breakdown voltage of InAlAs APDs is less temperature dependent compared to InP (Tan et al., 2010), which would be useful in temperature sensitive applications, thus making temperature control less critical.

The sensitivity performance criterion for digital receivers is its bit-error rate (BER), which is the probability of an error in the bit-identification by the receiver. The receiver sensitivity is defined as the minimum average optical power to operate at a certain BER; 10^{-12} being a common standard for digital optical receivers. The sensitivity of APD-based high speed optical receivers is governed by three main competing factors, namely the excess noise, avalanche-buildup time and dark current of the APD. Generally, the excess noise and avalanche-buildup time increases with APD gain. Thus, for a fixed multiplication layer thickness, there is a sensitivity-optimised gain that offers a balance between SNR while keeping the degrading contributions from the excess noise factor and intersymbol-interference (ISI) at a minimum. More importantly, changing the thickness of the multiplication layer strongly affects the receiver sensitivity, as the aforementioned three

factors change. Reducing the thickness of the multiplication layer serves to reduce the excess noise factor, due to the dead space effect, (Li et al., 1998) and minimise ISI via reducing carrier transit times across the avalanche region. On the other hand, the increase in the field in thin layers accentuates tunnelling currents at exponential rates (Forrest et al., 1980a). Thus, careful attention is required when determining the multiplication layer thickness for an optimum APD design.

It is, therefore, very useful and interesting to model the sensitivity of an APD-based receiver system accurately. Such models have been developed but none included some form of dark current mechanism, which can significantly affect the receiver's sensitivity. Characterisation of the APD excess noise factor in test structures is also necessary in order to model the BER of an APD-based receiver system. Several efforts have been made to systematically characterise promising detector material systems including InP and InAlAs.

In this chapter, we will describe the model used to investigate the receiver-sensitivity-optimisation of InP and InAlAs APDs, which include dark current contributions from tunnelling current. A comprehensive assessment of the measurement systems reported in the literature is also provided followed by two suggestions for an improved design. The results of the BER calculations on receiver systems using InP APDs will be presented, followed by a discussion on the competing effects of performance-determining factors. A straightforward comparison between InP and InAlAs APDs will then be presented with an analysis on the difference.

2. Impact ionisation

The impact ionisation process occurs when a carrier injected into a high-field region gains enough energy from the applied field and collides with the lattice structure to produce an electron-hole pair. In an electron-initiated process, as depicted schematically in Figure 1(a), an energetic electron at a higher state of the conduction band scatters with an electron at the top of the valence band via Coulombic interaction, and promotes it to the bottom of the conduction band (Singh, 1995). As this process can have a cascading effect, the net result is the creation of many secondary electrons and holes from a single primary electron, generated through absorption of a photon. A similar process occurs in hole-initiated impact ionisation with similar results, as shown in Figure 1(b).

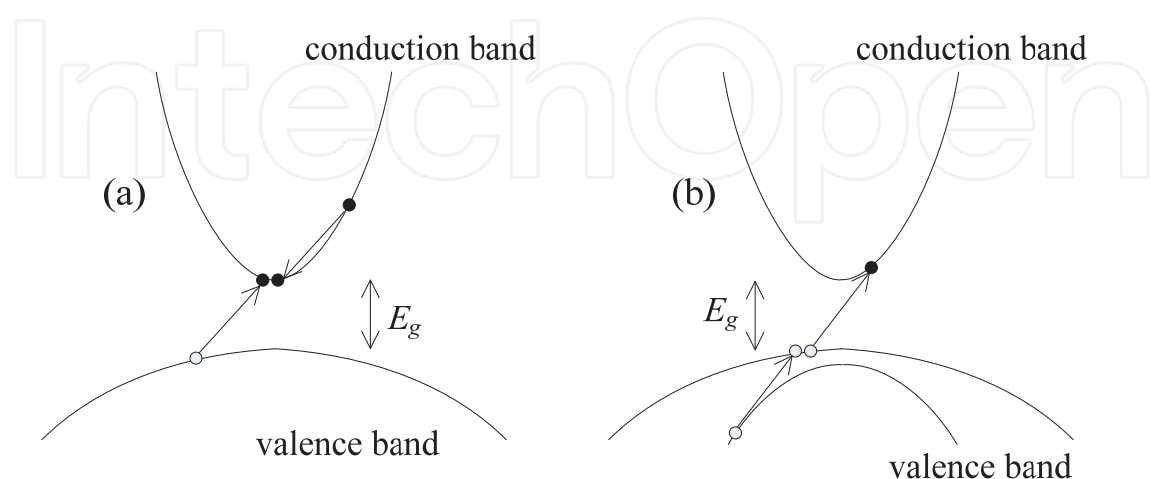


Fig. 1. Schematic wavevector diagrams depicting (a) electron-initiated and (b) hole-initiated impact ionisation events.

Due to conservation of energy and momentum, a threshold energy, E_{th} , prerequisite has to be satisfied by the primary carrier. This energy has to be greater than the band gap, E_g , as the carrier also experiences non-ionising collision processes such as phonon scattering, which involves carriers gaining energy, losing energy or exchanging momentum. On average, carriers will lose energy by phonon scattering because the emissive phonon scattering rate is proportional to n_p+1 whereas the phonon absorption rate is proportional to n_p , where n_p is the phonon occupation number, which depends on the phonon energy, $\hbar\omega$, given by $n_p = \frac{1}{\exp\left(\frac{\hbar\omega}{k_B T}\right) - 1}$, where k_B is Boltzmann's constant and T is the absolute temperature.

The generation rate or mean number of ionisation events per unit distance for a carrier is known as the impact ionisation coefficient. The electron and hole ionisation coefficients, α and β respectively, are functions of electric field, temperature and material.

Carriers with energy less than E_{th} are unable to initiate impact ionisation and have to traverse a distance, within the high electric field region, known as the dead space before they acquire sufficient energy. A carrier that has gained E_{th} is said to be *enabled*, as its ionisation probability is no longer zero.

The mean multiplication factor, M , or gain is the ratio of the total number of carriers generated to the number of carriers injected. In electrical current terms, this is given by $M = I_p/I_i$, where I_p is the generated output photocurrent (where carrier multiplication occurs) and I_i is the initial photocurrent (before carrier multiplication). M can be calculated using the local model (Stillman and Wolfe, 1977) where the multiplication layer width is assumed to be much greater than dead space. Neglecting dead space and solving electron and hole continuity current equations in the multiplication layer, M is given by

$$M(x) = \frac{\exp\left[-\int_0^x (\alpha(x') - \beta(x')) dx'\right]}{1 - \int_0^w \alpha(x') \exp\left[-\int_0^{x'} (\alpha(x'') - \beta(x'')) dx''\right] dx'} \quad (1)$$

where α and β are position-dependent ionisation coefficients, and electrons are injected from $x = 0$ and holes from $x = w$, i.e. electrons drift in the positive x direction, holes otherwise.

Assuming a uniform electric field, i.e. an ideal $p-i-n$ diode, α and β have no spatial dependence and (1) simplifies to

$$M(x) = \frac{(\alpha - \beta)e^{-(\alpha - \beta)x}}{\alpha e^{-(\alpha - \beta)w} - \beta} \quad (2)$$

Hence, pure electron mean multiplication factors, M_e and M_h , are given by

$$M_e = \frac{(\alpha - \beta)}{\alpha e^{-(\alpha - \beta)w} - \beta} \quad (3)$$

and

$$M_h = \frac{(\alpha - \beta)e^{-(\alpha-\beta)w}}{\alpha e^{-(\alpha-\beta)w} - \beta} \quad (4)$$

Rearranging equations #, a and β can be determined by measuring M_e and M_h in ideal $p-i-n$ structures, based on the simplified assumptions outlined above, as

$$\alpha = \frac{1}{w} \left[\frac{M_e - 1}{M_e - M_h} \right] \ln \left(\frac{M_e}{M_h} \right) \quad (5)$$

and

$$\beta = \frac{1}{w} \left[\frac{M_h - 1}{M_h - M_e} \right] \ln \left(\frac{M_h}{M_e} \right) \quad (6)$$

3. Excess noise

The stochastic nature of the impact ionisation process results in fluctuations in the multiplication factor. This noise, introduced by impact ionisation, is caused by the unpredictability in the production position of the secondary carrier.

For an APD under illumination, assuming the incident photons have a Poisson distribution generating a primary photocurrent, i_{pr} , in a circuit of bandwidth, B , the mean number of photogenerated carriers is given by

$$\langle m \rangle = \eta \phi T_c \quad (7)$$

where η is the quantum efficiency, ϕ is the photon flux in photons per second, and T_c is the collection time interval.

For a measurement circuit with bandwidth B , the minimum distinguishable time interval between received current pulses can be defined by the Nyquist criterion as $T_c = 1/(2B)$.

Hence, the total current collected in time interval, T_c , and the associated variance, are given by

$$\langle i_{pr} \rangle = \frac{e \langle m \rangle}{T_c} \quad (8)$$

and

$$\sigma_{pr}^2 = \left(\frac{e}{T_c} \right)^2 \sigma_{\langle m \rangle}^2 \quad (9)$$

where σ_{pr}^2 is the variance in photocurrent, $\sigma_{\langle m \rangle}^2$ is the variance in number of photogenerated carriers, e is the unit of electron charge. From (7) and (8), the mean photocurrent is, therefore, given by

$$\langle i_{pr} \rangle = e \eta \phi \quad (10)$$

and from (8) and (9), noting that $\langle m \rangle = \sigma_{\langle m \rangle}^2$ for a Poisson distribution of photons, the variance in photocurrent is given by

$$\sigma_{pr}^2 = 2e \langle i_{pr} \rangle B \quad (11)$$

These simplified derivations show that even without avalanche gain, variance in the photocurrent is expected due to the random nature of the photocurrent generation. Note, also, that (11) is identical to the shot noise formula for variance in a current.

Hence, for an APD considered as an *ideal noiseless multiplier* with multiplication, $\langle M \rangle$, the mean photocurrent, $\langle i_{ph} \rangle$, is given by

$$\langle i_{ph} \rangle = \langle i_{pr} \rangle \langle M \rangle \quad (12)$$

and the mean square noise current is given by

$$N_{ideal} = 2e \langle i_{pr} \rangle \langle M \rangle^2 B \quad (13)$$

Equation (13) describes the ideal (noiseless) multiplication process, where the stochastic nature of the avalanche multiplication process is excluded. To account for the noise associated with the multiplication process, the excess noise factor, F , is introduced into (13), giving

$$N = 2e \langle i_{pr} \rangle \langle M \rangle^2 BF \quad (14)$$

where F is expressed as

$$F = \frac{\langle M^2 \rangle}{\langle M \rangle^2} \quad (15)$$

Equation (15) shows that the average multiplication, $\langle M \rangle$, has statistical fluctuations and F in (14) describes how much the avalanche noise deviates from an ideal multiplier. When there is no multiplication noise, $F = 1$ and only shot noise exists. Hence, F permits the noise performance of APDs to be considered in the same terms as that of other system components.

4. The Random Path Length model

Unlike the local model described earlier, non-local models account for the dead space and one such model is the Random Path Length (RPL) model (Ong et al., 1998). The RPL model is a simple model that is able to predict multiplication and excess noise characteristics in APDs by modelling the transport of carriers during the impact ionisation process. The model operates by consideration of the ionisation path length probability distribution function, $P(x)$, for each carrier as it passes through the device. For the *hard threshold dead space model*, which is considered here, the probability for an electron to impact ionise for the first time after travelling a distance x in a uniform electric field, E , is given by

$$P_e(x) = \begin{cases} 0 & , x \leq d_e^* \\ \alpha^* \exp[-\alpha^*(x - d_e^*)] & , x > d_e^* \end{cases} \quad (16)$$

where α^* is the enabled electron ionisation coefficient and d_e^* is the electron hard threshold dead space, given by

$$d_e^* = \frac{E_{the}}{q\mathfrak{I}} \quad (17)$$

and E_{the} is the electron ionisation threshold energy, q is the electron charge and \mathfrak{I} is the applied electric field. From (16), the average distance between electron initiated ionising collisions is

$$\int_0^{\infty} xP_e(x) dx = \frac{1}{\alpha^*} + d_e^* \quad (18)$$

and the mean ionisation coefficient is the reciprocal of this, that is

$$\alpha = \frac{1}{d_e^* + \frac{1}{\alpha^*}} \quad (19)$$

From (16), the probability that a carrier travels a distance x without impact ionising is

$$S_e(x) = \begin{cases} 1 & , x \leq d_e^* \\ \exp[-\alpha^*(x - d_e^*)] & , x > d_e^* \end{cases} \quad (20)$$

Thus, a random electron ionisation path length, l_e , can be expressed by substituting uniformly distributed numbers, r , between 0 and 1 for $S_e(x)$ to give

$$l_e = d_e^* - \frac{\ln(r)}{\alpha^*} \quad (21)$$

Similar expressions for the hole impact ionisation path length can be obtained by substituting $P_e(x)$, $S_e(x)$, α , α^* , d_e^* and l_e with $P_h(x)$, $S_h(x)$, β , β^* , d_h^* and l_h , in (16)-(21).

The RPL simulation is composed of n number of trials, where the choice of n is a trade-off between accuracy and computation time. A trial in the RPL simulation is complete when all the carriers have left the multiplication region. Each injected carrier gives rise to a multiplication value, m , which is a random variable due to the stochastic nature of the impact ionisation process. The mean multiplication and excess noise factor can be calculated using

$$M = \frac{1}{n} \sum_{i=1}^n m_i \quad (22)$$

and

$$F = \frac{1}{nM^2} \sum_{i=1}^n (m_i^2) \quad (23)$$

where m_i is the multiplication resulting from trial i in the RPL simulation.

5. BER model

The current developed in an APD, by chains of impact ionisation events, take time to build up. Materials with disparate ionisation coefficients tend to have longer chains of ionisation events; thus having longer current buildup times compared to currents developed by shorter chains. This buildup time, which is stochastic, has an associated bandwidth limit and thus governs the APD speed and ultimately, the level of ISI in the receiver system.

To understand the stochastic nature of the APD buildup-time-limited bandwidth and its statistical correlation with the gain, Sun *et al.* introduced the *shot-noise equivalent bandwidth* (Sun et al., 2006), defined as $B_{\text{sneq}} = \langle M^2/T_{bu} \rangle / 2\langle M \rangle^2 F$, where T_{bu} is the avalanche buildup time. The quantity B_{sneq} is the bandwidth that, when used in the usual formula for APD-amplified shot noise, $\sigma^2 = 2e\langle M \rangle^2 F B_{\text{sneq}} \eta P/h\nu$, gives the correct value of the shot-noise variance, where η is the APD quantum efficiency, P is the optical power, h is Planck's constant, and ν is the photon's frequency. Due to the stochastic coupling between T_{bu} and M , B_{sneq} is generally greater than the conventional 3dB bandwidth of the APD, $B_{3\text{dB}}$, which is taken as the 3dB-drop point in the Fourier transform of the APD's mean impulse-response function. This discrepancy can be as high as 30%, leading to a similar error in the prediction of the APD-amplified shot-noise variance if $B_{3\text{dB}}$ is used in place of B_{sneq} .

The Gaussian-approximation method was used to calculate the BER and is described as follows. The output of the integrate-and-dump receiver was approximated by a Gaussian random variable with the exact mean and variance, and the BER was computed using (Agrawal, 1997)

$$\text{BER} \approx \frac{1}{4} \left[\text{erfc} \left(\frac{\theta - \mu_0}{\sqrt{2}\sigma_0} \right) + \text{erfc} \left(\frac{\mu_1 - \theta}{\sqrt{2}\sigma_1} \right) \right] \quad (24)$$

where μ_0 and σ_0^2 denote the mean and variance for the receiver's output conditional on the present bit (i.e., the information bit corresponding to the receiver's present integration period) being '0,' and μ_1 and σ_1^2 are similar quantities conditional on the present bit being '1.' The decision threshold, θ , is taken as

$$\theta = \frac{\mu_0\sigma_1 + \mu_1\sigma_0}{\sigma_0 + \sigma_1} \quad (25)$$

which is a convenient approximation to the optimal decision threshold that minimises the BER (Agrawal, 1997). The expressions for the parameters μ_0 , σ_0^2 , μ_1 and σ_1^2 are derived as (Sun et al., 2006)

$$\mu_0 = \frac{1}{2} \frac{n_0 \langle M \rangle}{\kappa\lambda} (1 - e^{-\kappa\lambda}) \quad (26)$$

$$\sigma_0^2 = \frac{1}{4} \frac{n_0^2 \langle M \rangle^2 (1 - e^{-\kappa\lambda})^4}{\kappa\lambda^2 (1 - e^{-2\kappa\lambda})} + \frac{n_0 \langle M \rangle^2 F}{2\kappa\lambda} (1 - e^{-\kappa\lambda} - \kappa\lambda e^{-\kappa\lambda}) + \sigma_J^2 \quad (27)$$

$$\mu_1 = \mu_0 + \frac{n_0 \langle M \rangle}{\kappa \lambda} (\kappa \lambda - 1 + e^{-\kappa \lambda}) \quad (28)$$

$$\sigma_1^2 = \sigma_0^2 + \frac{n_0 \langle M \rangle^2 F}{\kappa \lambda} (\kappa \lambda - 2 + 2e^{-\kappa \lambda} + \kappa \lambda e^{-\kappa \lambda}) \quad (29)$$

where n_0 is the average number of absorbed photons per '1' bit, $\kappa = 4B_{\text{sneq}}/2\pi B_{3\text{dB}}$ is the *bandwidth correction factor*, which accounts for the discrepancy between B_{sneq} and $B_{3\text{dB}}$, and λ , is the *detector-speed factor*, which is a measure of the detector's relative speed, defined as $\lambda = 2\pi B_{3\text{dB}}/R_b$, where $R_b = 1/T_b$ is the bit transmission speed, and T_b is the bit duration. Finally, the term σ_J^2 represents the variance of Johnson noise accumulated in the integration time. Note that μ_0 , σ_0^2 , μ_1 and σ_1^2 are quantities that are averaged over all possible past bit patterns.

The expressions in (26)–(29) are generalisations of the traditional expressions for the output statistics of APD-based receivers found in optical communication literature (Agrawal, 1997). Whilst these expressions capture the usual effects of shot noise and the excess noise due to avalanche multiplication, they additionally capture the effects of ISI, relative speed of the detector, as well as the stochastic coupling between the APD's gain and buildup time through the effective use of the parameters κ and λ . For an instantaneous detector, i.e. $B_{3\text{dB}} = \infty$, the detector-speed factor λ is infinite, and the expressions shown in (26)–(29) collapse to the traditional expressions for the receiver mean and variance in the absence of ISI (Agrawal, 1997): $\mu_0 = 0$, $\sigma_0^2 = \sigma_J^2$, $\mu_1 = n_0 \langle M \rangle$, and $\sigma_0^2 = \sigma_J^2 + n_0 \langle M \rangle^2 F$. Moreover, in detectors for which the gain is unity, e.g. a *p-i-n* diode, the bandwidth correction factor κ is unity, resulting in simplified versions of (26)–(29) that continue to capture the effect of ISI.

The term in μ_0 and the first two terms in σ_0^2 , as shown in (26) and (27), respectively, are due entirely to contributions from ISI resulting from the random stream of bits (preceding the present bit). In particular, they arise from contributions from photo-generated carriers generated within the bits that precede the present bit. The second term in (28) and second term in (29) are due to contributions from carriers generated during the present bit. The parameters μ_0 , σ_0^2 , μ_1 and σ_1^2 shown above do not include the contribution from the APD's tunnelling current generated in the multiplication region of the APD.

5.1 Variant of the Gaussian-approximation

In the previous section, it was assumed that the receiver output, conditional on the state of the present bit, is a Gaussian random variable. Ong et al. (Ong et al., 2009) replaced this with the more realistic assumption that the receiver output, conditional on the state of the present bit *and the entire past bit stream*, is a Gaussian random variable. This enables one to compute the BER conditional on the entire past bit stream, and then average the resulting pattern-specific BERs over all possible past bit patterns to obtain the overall average BER. The advantage of this approach is that it relaxes the often unrealistic assumption of a uni-modal probability density function for the receiver output conditional on the state of the present bit. While this variant approximation will yield an improved approximation of the average BER, it comes with a slight increase in computation.

The mean and variance of the ISI contributions in the receiver output from the k th past bit alone are respectively given by

$$\mu_{\text{ISI},k} = \frac{2n_0 \langle M \rangle e^{-\kappa\lambda k}}{\kappa\lambda} (\cosh(\kappa\lambda) - 1) \quad (30)$$

and

$$\sigma_{\text{ISI},k}^2 = \frac{n_0 \langle M \rangle^2 F}{\kappa\lambda} e^{-\kappa\lambda k} (e^{-\kappa\lambda} - 1) (1 - \kappa\lambda e^{-\kappa\lambda} - e^{-\kappa\lambda}) \quad (31)$$

Considering an arbitrary past bit pattern, I_j , of length L bits, the mean of the receiver output when the current bit is '0' can be calculated by adding up the contributions from each of the ISI terms from the past bits in the pattern I_j ; which yields the expression

$$\mu_0(I_j) = \sum_{k=1}^L a_k(I_j) \mu_{\text{ISI},k} \quad (32)$$

where $a_k(I_j) = 0$ unless the k th bit in the pattern I_j is a '1' bit, in which case $a_k(I_j) = 1$. Similarly, the variance of the receiver output associated with the pattern I_j when the current bit is '0' can be calculated by adding up the ISI contributions from past bits in the specific pattern as well as contribution from Johnson noise to obtain

$$\sigma_0^2(I_j) = \sum_{k=1}^L a_k(I_j) \sigma_{\text{ISI},k}^2 + \sigma_j^2 \quad (33)$$

5.2 Generalisation of the model to include tunnelling current

The un-multiplied band-to-band tunnelling current, I_{tunn} , is modelled by (Forrest et al., 1980b)

$$I_{\text{tunn}} = \frac{(2m^*)^{0.5} q^3 \mathfrak{Z} VA}{h^2 E_g^{0.5}} \exp\left(-\frac{2\pi\sigma_T (m^*)^{0.5} E_g^{1.5}}{qh\mathfrak{Z}}\right) \quad (34)$$

where m^* is the effective electron mass, V is the applied reverse bias voltage, A is the device area, and σ_T is the tunnelling fitting parameter. The average number of dark carriers generated per bit time interval, T_b , is given by $n_d = I_{\text{tunn}} T_b / q$. Since the dark-carrier generation has Poisson statistics, it is plausible to attempt to include the effect of dark carriers on the parameters μ_0 , σ_0^2 , μ_1 and σ_1^2 by treating dark carriers as photo-generated carriers.

The expression for $\mu_0(I_j)$ including dark carrier generation was obtained as

$$\begin{aligned} \mu_0(I_j) &= \sum_{k=1}^L a_k(I_j) \mu_{\text{ISI},k} + \frac{n_d \langle M \rangle}{\kappa\lambda} (1 - e^{-\kappa\lambda}) + \frac{n_d \langle M \rangle}{\kappa\lambda} (\kappa\lambda - 1 + e^{-\kappa\lambda}) \\ &= \sum_{k=1}^L a_k(I_j) \mu_{\text{ISI},k} + n_d \langle M \rangle \end{aligned} \quad (35)$$

while the expression for $\sigma_0^2(I_j)$ was derived as

$$\sigma_0^2(I_j) = \sum_{k=1}^L a_k(I_j) \sigma_{\text{ISI},k}^2 + \frac{n_d \langle M \rangle^2 F}{\kappa \lambda} (\kappa \lambda - 1 + e^{-\kappa \lambda}) + \sigma_f^2 \quad (36)$$

The receiver mean output, $\mu_1(I_j)$, when the present bit is '1' is obtained by adding to $\mu_0(I_j)$ the contributions from the photons in the current bit. Combining this component with the contributions from the ISI terms gives

$$\mu_1(I_j) = \mu_0(I_j) + \frac{n_0 \langle M \rangle}{\kappa \lambda} (\kappa \lambda - 1 + e^{-\kappa \lambda}) \quad (37)$$

Similarly, adding the contributions from the photons in the current bit to $\sigma_0^2(I_j)$ yields

$$\sigma_1^2(I_j) = \sigma_0^2(I_j) + \frac{n_0 \langle M \rangle^2 F}{\kappa \lambda} (\kappa \lambda - 2 + 2e^{-\kappa \lambda} + \kappa \lambda e^{-\kappa \lambda}) \quad (38)$$

Finally, for every past bit pattern I_j , $j = 1, \dots, 2^L$, the *pattern-specific* BER can be calculated as follows

$$\text{BER}(I_j) \approx \frac{1}{4} \left[\text{erfc} \left(\frac{\theta - \mu_0(I_j)}{\sqrt{2} \sigma_0(I_j)} \right) + \text{erfc} \left(\frac{\mu_1(I_j) - \theta}{\sqrt{2} \sigma_1(I_j)} \right) \right] \quad (39)$$

where θ is calculated as before from (25). To calculate the overall BER, the ensemble average of the pattern-specific BER is computed over all possible past bit patterns; more precisely,

$$\text{BER} = \frac{1}{2^L} \sum_{j=1}^{2^L} \text{BER}(I_j) \quad (40)$$

The bit-length parameter, L , can be chosen to be sufficiently large to capture all significant ISI terms; in this work, $L = 10$ was found to be an adequate choice beyond which no significant change in the BER was observed.

6. Measurement of excess noise: A survey

Estimation of the BER, which can be obtained from a certain diode fabricated from a particular material system, relies on the characterisation of the excess noise factor using one or more test structures. The test structure is often a *p-i-n* avalanche photodiode into which light is injected through one of the contacts. To permit this injection, the shape of that contact is often an annulus. Generally many such characterisation diodes are fabricated simultaneously using standard optical lithographic and etching techniques. The excess noise power as a function of multiplication is measured for many values of multiplication such that the value of McIntyre's k_{eff} (McIntyre, 1966) for a particular material system can be established. This value can then be used in conjunction with the methods described herein and noise analyses of the front end receiver circuits to estimate the BER for a specified optical irradiance. In this section we consider each of the noise measurement systems reported in the literature and offer two suggestions for an improved system.

Several excess noise measurement systems have been reported in the literature and comparisons between the circuits described may be drawn. The figures of comparison are,

- The system signal to noise ratio, where the signal is defined as full shot noise exhibited by $1\mu\text{A}$.
- The maximum permissible APD junction capacitance. In the case of multi-frequency systems the lowest available frequency is used; this produces the most favourable result. It is assumed that the system input impedance and diode junction capacitance form a first order low pass network.

6.1 Measurement systems

The first report of noise measurements on photodiodes was by Baertsch (1966). Insufficient information is provided to estimate this system's figures of merit so it is excluded from the comparison. Xie et al. (1993) proposed a measurement system that was substantially similar to Toivonen et al. (1992). The Xie et al. (1993) system represents both. Bulman (1983), Ando and Kanbe (1981) and Lau et al. (2006) presented systems based on phase sensitive detection. Xie et al. (1993) and Toivonen et al. (1992) used a DC approach.

6.1.1 Bulman's system

Figure 2 shows the system reported by Bulman (1983). It is a PSD system in which photocurrent and excess noise are extracted and read out by two lock in amplifiers. The APD is loaded by the AIL13680 through the bias tee. It may be assumed that the APD experiences a 50Ω load. The preamplifier output is fed to a receiver having a calibrated bandwidth. The resulting signal proportional to the noise power contained within the calibrated bandwidth is passed to a lock-in-amplifier.

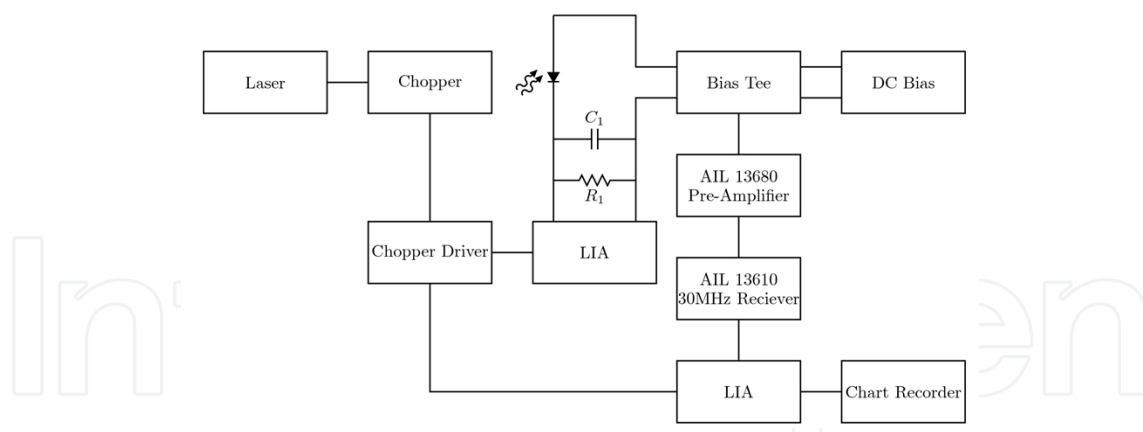


Fig. 2. Bulman's excess noise measurement system

Bulman proposes two methods to quantify the absolute noise power measured. Firstly a *p-i-n* detector is illuminated under unity gain conditions. It is assumed that under these conditions the system will measure full shot noise. A second calibration method is proposed in which a calibrated oscillator is used in place of the APD. This allows the experimenter to set the power which will be measured. Adjusting the power supplied by the oscillator allows the linear range of the system to be estimated. Bulman reports a 30dB range of linear measurement between -140dBm (10^{-17} W) and -110dBm (10^{-14} W). In several III-V semiconductors the impact ionisation coefficients are nearly equal. Under this assumption,

Tager (1965) has shown that excess noise is proportional to M^3 . Assuming Bulman's system is used from unity gain with a noise power of -140dBm the maximum multiplication prior to the limit of linearity in noise measurement is ten.

Bulman's report lacks some information regarding the front end amplifier. An Analog Devices AD9618 low noise opamp in non-inverting mode is used as a model. It achieves a gain of 100V/V and a bandwidth of 80MHz with 50Ω input impedance. The equivalent input noise voltage is 1.94 nV/Hz^{1/2}. Using this model as an approximation the signal-to-

noise ratio for Bulman's system is $SNR = \frac{(100 \times 50)^2 \times 2qi_{ph}}{(1.94 \times 10^{-9} \times 100)^2} = -36.73 \text{ dB}$. When $i_{ph} = 1\mu\text{A}$.

The capacitance of the diode which can be tolerated by Bulman's system is given to a first approximation by considering the system input impedance and the junction capacitance as a first order RC network. Assuming that all other parasitic effects (for example diode series resistance) are negligible in comparison, applying the commonly known expression for a first order network yields, $C = \frac{1}{2\pi fR}$, where $f = 30\text{MHz}$ and $R = 50 \text{ ohms}$. $C = 106\text{pF}$.

6.1.2 The PSD system of Ando and Kanbe

Ando and Kanbe (1981) reported the system shown in Figure 3. It is a PSD system in which the APD is loaded by 50Ω due to the input impedance of the IF amplifier. The measurement system bandwidth is defined by the IF amplifier and is 1MHz centred on 30MHz. The APD is biased using a bias tee and a variable voltage source. The noise power is read out from a lock in amplifier. A power meter and signal generator, with its output passed through a calibrated attenuator, provides a means of relating the absolute signal power to the value measured leaving the IF amplifier. Photocurrent is extracted by DC measurement of the current entering the bias tee. The measurement of devices exhibiting high dark current is therefore difficult with this system. The various connections required to calibrate the system and perform measurements are made using relays.

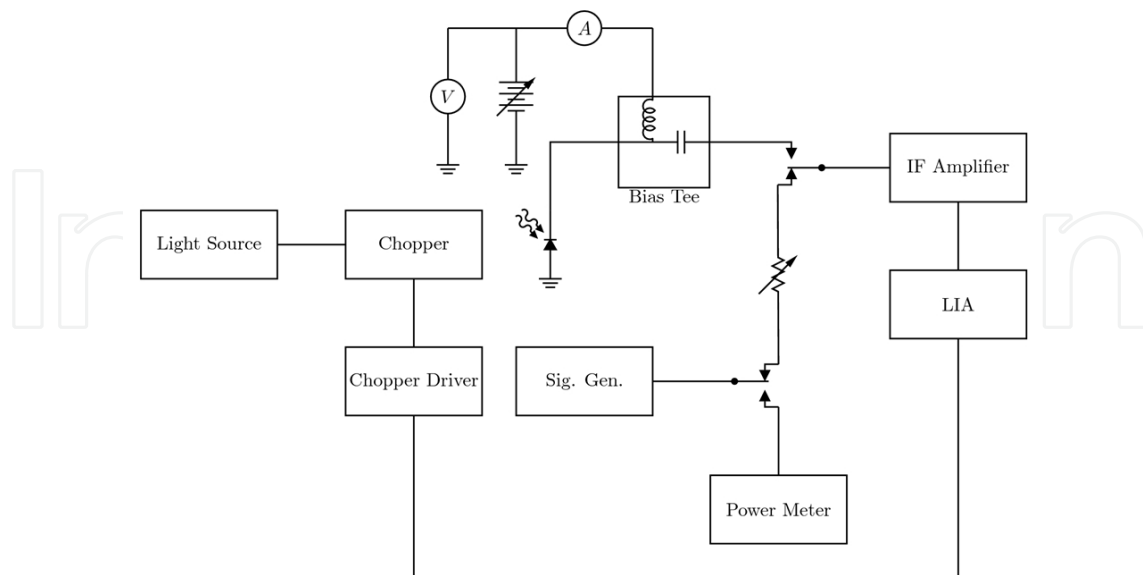


Fig. 3. The PSD noise measurement system due to Ando and Kanbe

Ando and Kanbe did not report any attempts to measure shot noise on their system. They also do not give information regarding the model numbers or manufactures of their system

components. No noise specifications for the instrumentation are given. Assuming that their system adds no noise other than the thermal noise of the 50Ω input impedance within the measurement bandwidth then the signal-to-noise ratio can be computed using

$$\text{SNR} = \frac{2qi_{ph}BR_{in}}{4k_B T \frac{B}{R_{in}}}, \text{ where } R_{in} = 50\Omega, B = 1\text{MHz}, T = 300^\circ\text{K and } i_{ph} = 1\mu\text{A. The junction}$$

capacitance which can be tolerated by Ando and Kanbe's system is calculated in a similar way to Bulman's system and produces the same answer $C = 106\text{pF}$.

The authors claim that noise power as low as -130dBm/Hz can be measured with 0.5dB accuracy. This represents a current of $0.125\mu\text{A}$ developing full shot noise.

6.1.3 A measurement after Xie et al.

The system proposed by Xie et al. (1993) is similar to that proposed by Toivonen et al. (Toivonen et al., 1992). The APD is connected to a micro-strip line and DC voltage is applied via a bias tee.

The measurement is made using a CW light source and a noise figure meter such as the Hewlett Packard 8970A. The system has two significant advantages over PSD systems such as those of Bulman (1983) and Li (Lau et al., 2006). Several measurement frequencies are available up to the limit of the circuits or analyser. Presently Agilent Technologies manufactures noise figure meters capable of measuring 10MHz to 26GHz with variable effective measurement bandwidth. This upper limit can be increased by using heterodyne methods. Xie's system (Xie et al., 1993) was limited to 1.3GHz maximum measurement frequency and 4MHz noise measurement bandwidth. The measurement is, in principle, quicker than a PSD system. The operation of PSD is discussed fully elsewhere (Horowitz and Hill, 1989) but it is sufficient to realise that the time constant of a PSD measurement may be expected to be longer than of a noise figure meter. DC measurements have several disadvantages over PSD however. For example the lowest practically measurable photo-generated noise is higher in CW systems than in some PSD systems. Using a transimpedance amplifier, Li (Li, 1999, Li et al., 1998) has shown that the transimpedance amplifier reported by Lau et al. (2006) can be used as the basis of a noise measuring system with greater (less negative) noise signal to noise ratio than is possible by using a 50Ω measurement system. A further objection to CW systems is that the noise without illumination - the dark noise - should be periodically measured in order to maintain consistency. The dark noise should be stable and sufficiently small, compared to the noise with illumination - combined light and dark noise - that the noise with illumination is dominated by the light noise. If this condition is not met the confidence of the measurement is compromised. Xie et al. (1993) reported measuring noise power as low as -182dbm/Hz without difficulty using the CW system shown in Figure 4. In a 50Ω system -182dbm/Hz is equivalent to full shot noise generated by $8\mu\text{A}$ of photocurrent. The capacitance which can be tolerated by this measurement system is computed at the lowest useable frequency, as this produces the most favourable result. By the same first order approximation used in Bulman's and Ando and Kanbe's systems Xie's system will exhibit a -3dB (half power) bandwidth of 10MHz when loaded with 636pF .

6.1.4 A PSD system after Li et al.

The system of Li (Lau et al., 2006, Li, 1999) employs phase sensitive detection and a transimpedance amplifier. A schematic diagram is shown in Figure 5.

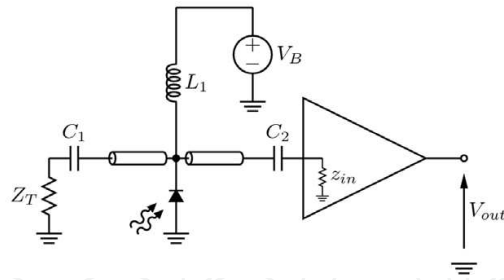


Fig. 4. CW excess noise measurement system after Xie et al.

The laser is chopped by mechanical means at 180Hz and is presented to the diode via a system of optics which is not shown. The TIA is used to convert the diode current into a voltage. This voltage is amplified using a commercial low noise wide band amplifier module (Minicircuits ZFL-500). A precision stepped attenuator (HP355D) is used to vary the system gain permitting measurement of high and low noise devices. The noise signal is separated from the low frequency component of the photocurrent by a Minicircuits SBP-10.7+ LC ladder filter which also defines the noise measurement bandwidth. After filtration, the signal resembles an amplitude modulated noise waveform, where periods of diode illumination produce greater noise amplitude than periods of darkness. Further amplification follows, prior to a wide band squaring and averaging circuit. The output of the squaring and averaging circuit is an approximately square voltage signal, the amplitude of which is proportional to the noise power contained in the measurement bandwidth. The fundamental frequency of the noise power signal is 180Hz. The squaring circuit is based on an Analogue Devices AD835 analogue multiplier. The averaging circuit is a first order RC filter with a time constant of approximately 100 μ s. The output from the squaring and averaging circuit is measured using a lock-in-amplifier. The photocurrent signal is taken from an auxiliary output of the TIA where the amplitude of the 180Hz square wave is proportional to the photocurrent. The photocurrent signal is measured on a second lock-in-amplifier.

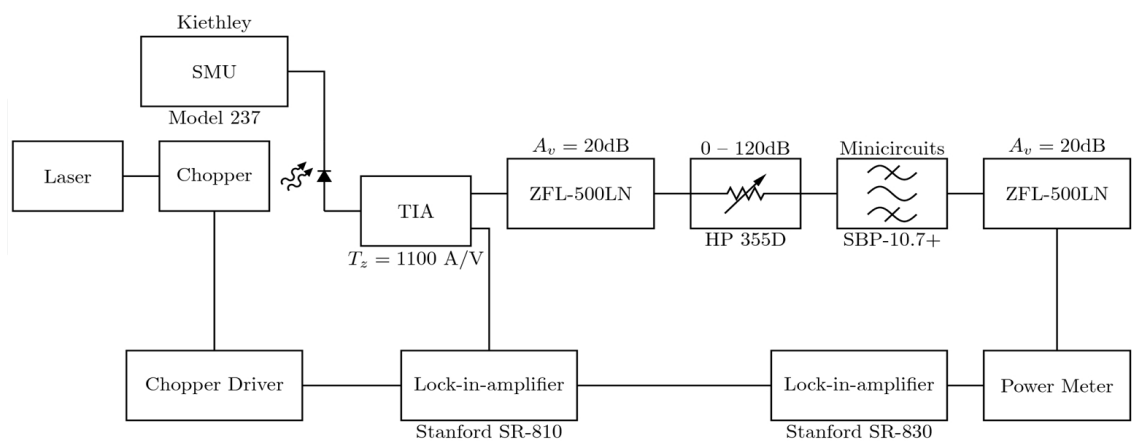


Fig. 5. Schematic diagram of an excess noise measurement system after Li

The system after Li (Lau et al., 2006, Li, 1999) is superior in noise performance to prior reported systems. The transimpedance amplifier provides a signal to noise ratio which is superior to that possible in a 50 Ω system. Consider the connection of a photodiode and a 50 Ω resistor. Assume that full shot noise generated by $i_{ph} = 1\mu$ A flows through the resistor

which exhibits thermal noise at $T = 300^\circ\text{K}$. The noise signal to noise ratio is then,

$$\text{NSNR} = 20 \log_{10} \frac{50 \sqrt{2q i_{ph}}}{\sqrt{50 \times 4k_B T}} = -30.15 \text{ dB}.$$

The noise signal to noise ratio (also considering $1\mu\text{A}$ photocurrent) of Li's system is -25.7dB (Li, 1999).

The dynamic range of Li's system is limited at the lower bound by the ability of the lock in amplifier to extract the in-phase excess noise signal from the system's background noise. Practical experimentation by the authors and their colleagues has shown that full shot noise developed by $1\mu\text{A}$ is approaching the limit and the shot noise from $0.1\mu\text{A}$ is not reliably measurable. The precise limit is difficult to quantify because it is affected by the prevailing electromagnetic conditions both radiated (passing through the experiment volume) and conducted into the power supply lines. At the upper bound the maximum attenuation of the stepped attenuator provides a limitation however more attenuation could be added without difficulty. The linearity of the transimpedance amplifier at high input current is a second limit. When driven from $\pm 5\text{V}$ supplies a TIA with a gain of 2200V/A will saturate at approximately 2.25mA input current. Because the relationship between excess noise factor and photo-multiplication varies between material systems it is unwise to speculate the maximum multiplication which can be used. Furthermore if a device is available which can be operated with a very large gain the optical illumination may be reduced in order to reduce the multiplied photocurrent and the excess noise power. In this way higher multiplication values may be measured. In order to measure lower multiplication values a larger primary photocurrent is required. By performing two or more measurements with differing primary photocurrents it is possible, assuming the APD is sufficiently robust, to measure multiplication and excess noise power over any desirable range above the system limit.

The capacitance tolerated by Li's transimpedance amplifier (Lau et al., 2006, Li, 1999) is lower than all of the other systems. The interaction of the APD junction capacitance and the feedback capacitor permits the existence of resonance in the transimpedance amplifier. When the capacitance is sufficiently large oscillation breaks out and the measurement system is saturated. There limit of measureable junction capacitance is however not governed by the presence of oscillation. A result of the interaction of the diode junction capacitance and the feedback capacitance is a dependence of the effective noise power bandwidth of the system on the diode junction capacitance, which is itself dependant on the DC bias voltage applied to the APD. As a result a correction to the measurement bandwidth must be made when processing the measurement data. The limitation of the measurable device capacitance is governed by the quality of the correction which can be achieved and by the presence of oscillation. While it is known that up to 56pF does not cause oscillation, Li placed the limit at 28pF (Li, 1999). This limit was obtained by calibrating the bandwidth of the transimpedance amplifier with several values of capacitance. Having performed the calibration, shot noise due to photo-generated carriers was measured using a unity-gain silicon photodiode. A second data set was gathered in which extra capacitance was placed in parallel with the photodiode to simulate a diode of greater capacitance. The simulated higher capacitance shot noise data was processed using the original calibration. The quality of the fitting of the standard photodiode shot noise and the simulated extra capacitance shot noise data was used as a basis for defining the quality of the correction and hence the maximum capacitance.

6.2 An improved CW noise measurement

We propose two possible improvements to the design proposed by Xie et al. (1993). Both are essentially improvements to the method by which the instrumentation is calibrated. The introduction of a calibrated noise source (HP346B) permits the use of direct noise figure measurement - as opposed to hot/cold measurements, which is a considerable improvement. The noise figure meter (N8973A, or an older model such as the N8970) is designed such that the noise source is connected to the device (for example an LNB) under test. Of course if the device is an electro-optical transducer this is impossible as there is no place to attach the noise source. This leads to the use of a pre-test calibration followed by hot/cold measurements. It would be preferable to use the noise figure analyser (NFA) according to its design principle, i.e. with the noise source in the measurement. The NFA is provided with prior calibration - by the manufacturer - of the noise source's contribution to the system. The system gain is also computable by measuring the effect on the noise output when the noise source is switched on and off - it is pulsed by the NFA. The time average of the change in noise level can provide the gain from the noise input port to the NFA input port. The prior knowledge of the known noise input from the calibrated source (HP346B) allows the NFA to compute the gain and noise figure nearly instantly, a considerable improvement in measurement speed, accuracy and precision. The question is then "How can the noise source be applied to the APD?" It cannot be directly applied. However, a secondary port can be created which permits the connection of an APD and the noise source to the NFA simultaneously. We provide two example designs here, the first uses a 50Ω matched topology similar to that of Xie et al. (1993). The second describes a similar overall structure but using a commercial transimpedance amplifier.

The APD multiplication, excess noise factor and noise power bandwidth can be established simultaneously in one measurement. The limitation of the system bandwidth can be alleviated by two methods. Firstly a higher maximum frequency noise figure meter can be obtained. Agilent Technologies presently manufactures noise figure meters/analysers capable of directly measuring up to 26GHz. The use of heterodyne techniques could extend this considerably. However a relatively inexpensive alternative is to use a lower bandwidth noise figure meter but begin measuring bandwidth once the APD has been biased to achieve a high gain. The high frequency roll off due to a finite gain bandwidth product can be observed at lower frequencies; the unity noise gain bandwidth product can then be inferred. The importance of correct impedance matching cannot be overemphasized.

6.2.1 50Ω system

The system diagram in Figure 6 shows the structure of the measurement setup. A Source-Measure Unit¹ drives a bias tee composed of L_1 and C_1 . An example of a suitable tee is the PicoSecond Model 5541A. The APD is connected to a microwave DC block (C_1) and this is in turn connected to a termination (50Ω). The DC block and the termination must be electrically close to the APD even at the highest measurement frequency. It is preferable to fabricate the DC block and the 50Ω termination with the APD as an integrated circuit. From the point of view of the first amplifier the APD is a Norton source coupled to the end of a properly terminated transmission line. Approximately half of the noise power will escape to ground via R_1 , the rest will enter the measurement system. It is possible to calibrate the

¹ A precision voltage source and current measuring device, e.g. Keithley models 237, 2400 and 2612

measurement system either manually (i.e. use a 50 Ω signal generator to list a table of adjustments for each frequency and post process the measured device data based on these reading) or automatically by using the HP 346B Noise source connected to the first amplifier input instead of the APD. The attenuator setting must be noted down when the calibration is carried out. The first amplifier in the chain must be of the lowest possible noise. Examples include Minicircuits ZFL-1000LN+, ZX60-33LN+ and Pasternack PE1513. The ZFL-1000 has low noise and a reasonably flat gain vs. frequency profile from 100kHz to 1GHz however bandwidth is limited to 1GHz. The ZX60-33LN+ has exceptionally low noise, and reasonable gain vs. frequency characteristics from 50MHz to 3GHz. The PE1513 has relatively poor noise especially as frequency increases, the gain vs. frequency profile is not ideal either; however it is the only device which covers the whole frequency range of the NFA, which is 3 GHz in the case of the N8973A. Unless APDs possessing bandwidths below 50MHz are to be routinely measured the authors preferred choice is the ZX60-33LN.

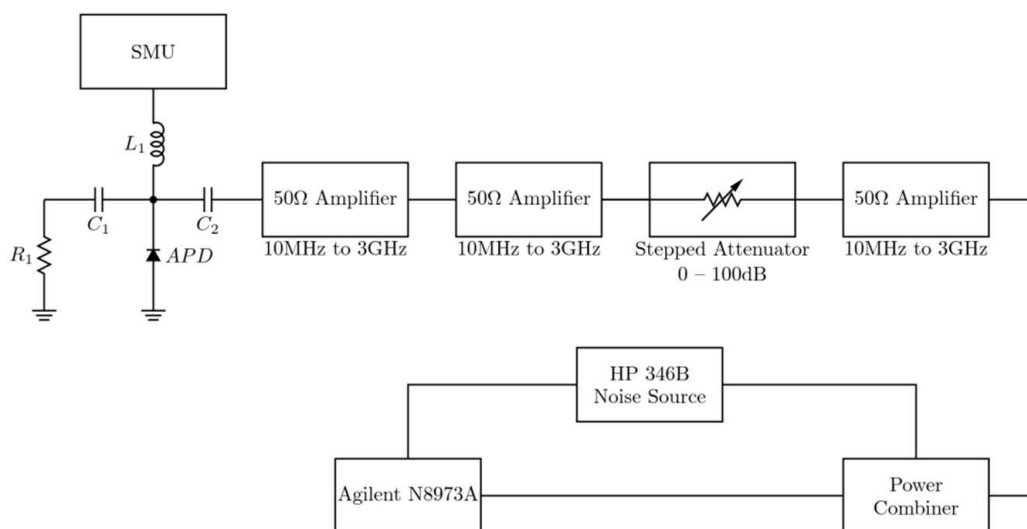


Fig. 6. 50 Ω 10MHz to 3GHz excess noise measurement system

The specifications of the second and third amplifiers are considerably less critical than the first. Any microwave device with reasonable noise and gain vs. frequency characteristics will be acceptable. The stepped attenuator should be of the precision type for example the Trilithic RSA35-100 (0dB to 100dB in 10dB steps) would be ideal. The power combiner may be of any type which covers the required bandwidth. A suitable resistive splitter/combiner is the Minicircuits ZX10E-14-S+.

The maximum device capacitance is approximately 2pF to obtain a 3dB point of approximately 3GHz. R_1 must be electrically close to the APD, consequently it is unlikely that the noise contribution of this resistor could be minimised by cooling as was reported by Xie et al. (1993). If the APD was measured at low temperature however it would be plausible to place R_1 and C_1 in the cryostat chamber with the APD, thus obtaining a noise advantage at lower temperatures. A laser is often used to excite electro-optical transducers in characterisation experiments. In this case the laser should be a gas laser possessing a single longitudinal mode, preferably frequency and amplitude stabilised. The authors have met with little success in noise characterisation experiments using semiconductor lasers, the laser relative intensity noise (RIN) is often too great to permit measurement of the detector noise.

6.2.2 TIA CW noise measurement system

The structure of this measurement system is nearly identical to the 50Ω system previously described. The principle difference is the use of a transimpedance amplifier front end instead of a 50Ω system. Figure 7 shows the system diagram.

C_1 provides an AC ground for the APD such that the very great majority of the noise current flows into the TIA. Example TIAs are given in the figure. Commercial TIAs often have input impedance which is not a good approximation to a virtual earth. As a result the maximum permissible device capacitance is often lower than in the 50Ω system case, and is dependent on the particular TIA in use. The MAX3910 provides $\sim 9\text{GHz}$ small signal bandwidth and nearly linear output voltage to input current relationship for photocurrents in the range 0 to $900\mu\text{A}_{\text{pk-pk}}$. The small signal gain of this TIA is approximately 1.6kV/A in the linear region.

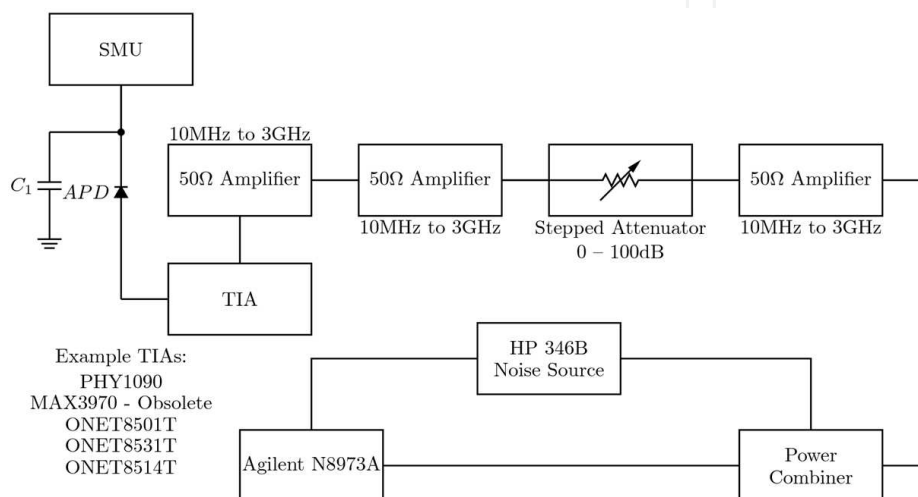


Fig. 7. Transimpedance amplifier excess noise measurement system

Unlike the 50Ω system it is not possible to connect the noise source to the TIA input for calibration purposes. Impedance matching considerations preclude it. This is a major limitation of the TIA measurement compared with the 50Ω measurement. Calibration of the TIA signal path with the noise source is only possible at the TIA output. A plausible method of calibration is to use a unity gain wide band *p-i-n* diode which is known to exhibit shot noise. Any deviation from shot noise can be calibrated out.

7. 10 Gb/s optical communications receiver BER analysis

This section will use the model described in section 3 to analyse the sensitivity of an APD-based receiver system by first investigating the performance of a 10 Gb/s receiver system using InP APDs followed by a discussion on the competing effects of excess noise, APD bandwidth, and tunnelling current on the receiver sensitivity. Similar calculations will then be performed for systems using InAlAs APDs to provide a straightforward and fair comparison with InP.

7.1 Parameters and coefficients

The non-local impact ionisation coefficients and threshold energies of Tan et al. (2008) for InP and Goh et al. (2007a) for InAlAs are used due to the extensive electric field range over which they are valid. The un-multiplied tunnelling current (Forrest et al., 1980b) defined by Equation (34) will use reported experimental InP (Tan et al., 2008) and InAlAs (Goh et al.,

2007b) tunnelling fitting parameters. Since the tunnelling fitting parameters vary with avalanche width, the lowest value, 1.16 for InP and 1.26 for InAlAs, was used for all investigated avalanche widths to assume the worst case scenario. The Johnson noise due to the TIA in the receiver at 10 Gb/s was assumed to be 636 electrons per bit, corresponding to an input noise current density of 10.7 pA/Hz^{1/2}. Calculations were performed for a series of InP and InAlAs APDs, with active area radius of 15µm and avalanche widths ranging from 0.1 to 0.5µm. A complete list of the parameters used in this section is shown in Table 1.

Parameters	InP	InAlAs
$v_e (\times 10^5 \text{ m/s})$	0.68	0.68
$v_h (\times 10^5 \text{ m/s})$	0.7	0.7
$E_{\text{the}} (\text{eV})$	2.8	3.2
$E_{\text{thh}} (\text{eV})$	3.0	3.5
$E_g (\text{eV})$	1.344	1.45
m^*	$0.08m_o$	$0.07m_o$
σ_T	1.16	1.26

Table 1. Parameters used to simulate the receiver sensitivity performance of InP, InAlAs, and InP and InAlAs APDs.

7.2 InP APD optimisation

Sensitivity versus gain curves were calculated for the InP APDs and the results are shown in Figure 8. The key observation is that for each APD, there exists an optimum mean gain that achieves the lowest sensitivity. In Figure 9, the optimum sensitivity for each device and corresponding mean gain are plotted as functions of the avalanche region width. This allows identification of the optimum avalanche width for a given transmission speed, thereby yielding the optimised sensitivity for a given transmission speed; in this case, 10 Gb/s. The calculations predicted an optimum avalanche width of 0.19 µm for InP APDs, yielding a sensitivity of -28.1 dBm at a gain of 13 for a 10 Gb/s system.

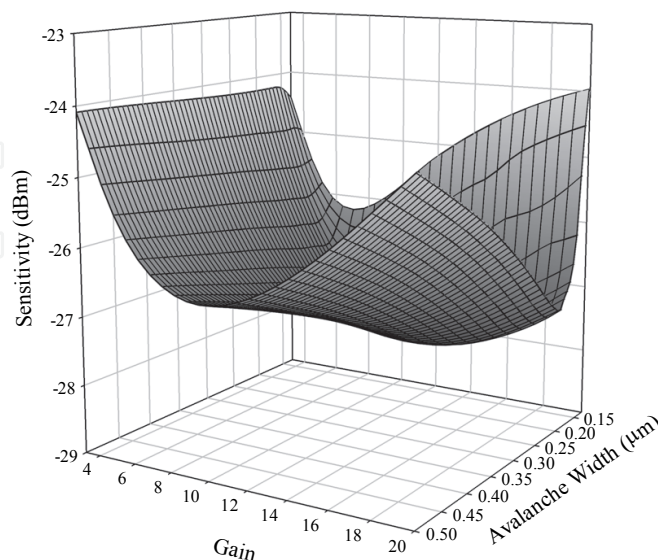


Fig. 8. Receiver sensitivity versus gain for the InP p-i-n APDs, of different avalanche widths, investigated for a 10 Gb/s transmission system.

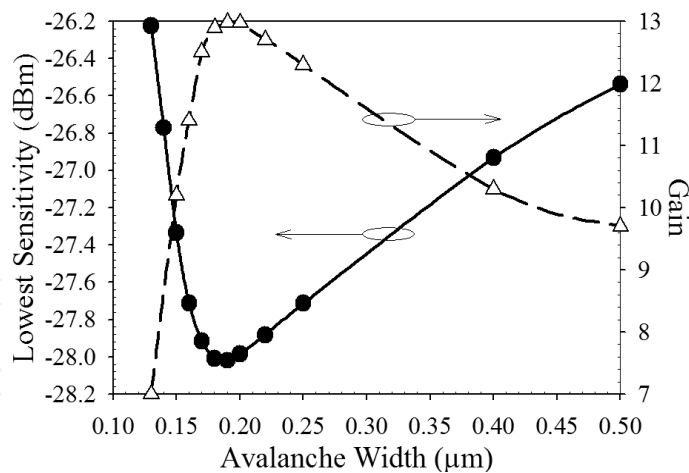


Fig. 9. Lowest sensitivity (solid line, left axis) and its corresponding optimal mean gain (dashed line, right axis) versus InP APD avalanche width for a 10 Gb/s transmission system.

7.3 Competing performance-determining factors

In order to independently assess the significance of (i) ISI, (ii) device bandwidth, and (iii) tunnelling current, three additional sets of calculations were carried out, which shall be referred to as *incomplete* calculations (all at 10 Gb/s). Each set in the incomplete calculations ignores one of the aforementioned three effects. ISI is excluded from the calculations by setting $L = 0$ in (35) and (36). The device bandwidth constraint is removed by setting $\lambda = \infty$, which corresponds to an instantaneous APD. The effect of ISI is also automatically ignored in an instantaneous APD. It is important to note that when ISI is excluded from the model by means of setting $L = 0$, the receiver output is still affected by the bandwidth through the parameter λ in the second terms of (37) and (38), which in turn, represent the attenuation in the receiver output resulting from the APD's bandwidth constraint. This shows the capability of the model to exclude ISI effects alone without the need for assuming an infinite APD bandwidth. Tunnelling current is excluded by setting $n_d = 0$.

Results from each of these three sets of incomplete calculations are compared to those from the *complete* calculation in Figure 10. By observing Figure 9, it is clear that the optimum sensitivity versus width characteristic for a given transmission speed is controlled in a very complex fashion by three device-related factors, namely the tunnelling current, excess noise, and device bandwidth. As the device width decreases, the operating field increases, resulting in increased tunnelling current. The excess noise also decreases with thinner devices confirming, as the dead-space effect becomes more significant (Tan et al., 2008, Forrest et al., 1980a). At the same time, the APD's bandwidth decreases with w ; this causes weaker receiver output as well as an increase in the significance of ISI, thereby causing an elevation in the sensitivity.

For the complete calculation results, high sensitivity values for diodes narrower than the optimum avalanche width optimum are due to high tunnelling current. For diodes wider than the optimum avalanche width, sensitivity increases with w , as described above. However, the relative dominance of increasing k_{eff} (resulting in an increase in the excess noise) and decreasing diode bandwidth becomes clear through careful observation of the incomplete calculations. Sensitivity results from the calculations that exclude the bandwidth constraint are only affected by changes in the excess noise when w is increased beyond the

optimum width. Consequently, the sensitivity is observed to increase more slowly with avalanche width compared to that obtained from the complete calculation, suggesting that a decreasing device bandwidth plays a more dominant role than increasing excess noise on sensitivity as w increases. As such, calculations that ignore bandwidth effects will erroneously predict higher optimal device gains compared to those predicted by the complete calculation.

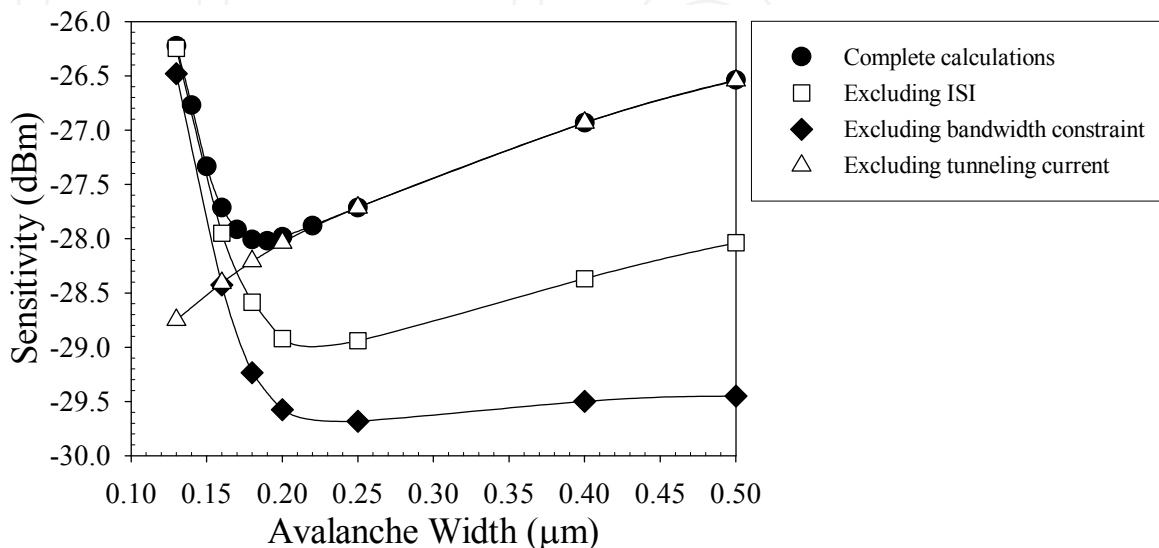


Fig. 10. Sensitivity versus avalanche width for the complete and various incomplete calculation conditions for a 10Gb/s system. Different curves identify the distinct roles of ISI, device bandwidth, avalanche excess noise, and tunneling current.

7.4 Comparison of InP and InAlAs APDs

The optimum sensitivity (optimized over the mean gain) and its corresponding mean gain from the InP and InAlAs calculations are plotted against the avalanche region width, as shown in Figure 11, for a 10 Gb/s system. The calculations predict an optimum w of 0.15 μm, with sensitivity of -28.6 dBm and gain of 15, for InAlAs APDs in a 10 Gb/s system.

For any given width, InAlAs provides better sensitivity than InP. However, the improvement is not significant. At their respective optimum avalanche widths, the difference in receiver sensitivities is only 0.5 dBm at both transmission speeds, corresponding to a reduction of 11% in optical signal power at the receiver input. This marginal improvement was also reported by Marshall et al. (2006) albeit with higher sensitivity values, as a result of ignoring the effects of APD bandwidth and ISI. The modesty in this improvement is partly due to a diminishing advantage, as w decreases, in excess-noise characteristics in InAlAs over InP, as shown in Figure 11 in the form of effective ionization coefficient ratio, k_{eff} . At the optimum avalanche widths, the values for k_{eff} are 0.21 and 0.29, for InAlAs (at 0.15 μm) and InP (at 0.18 μm), respectively. Another factor is the slightly higher gain-bandwidth product in InAlAs compared to InP, 220 and 180 GHz, respectively, at their optimum widths, as shown in Figure 11. The slightly lower tunnelling current in InAlAs APDs compared to those in InP APDs (expected from the slightly larger bandgap of InAlAs), also shown in Figure 11, also contributes slightly to the improvement in receiver sensitivity.

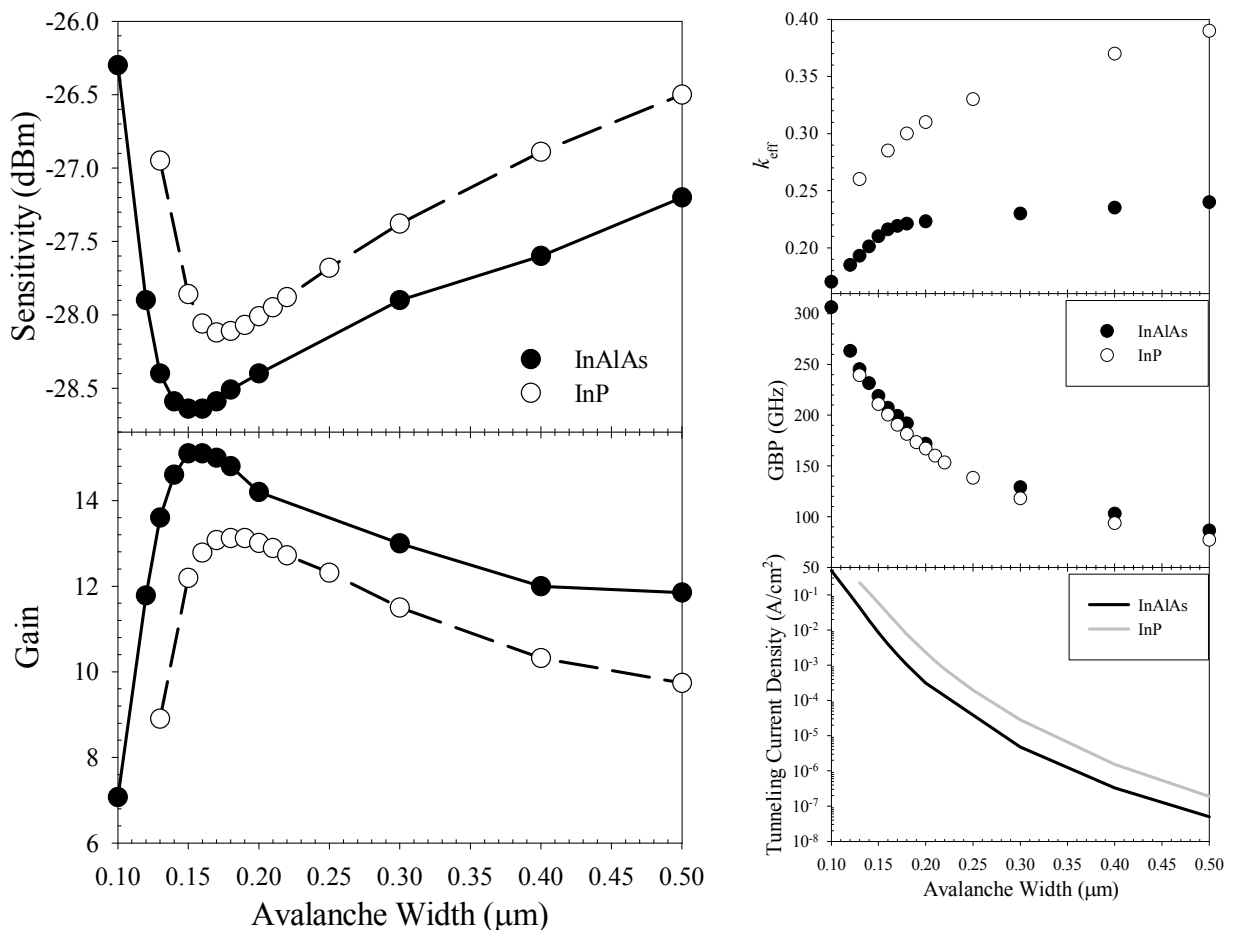


Fig. 11. Optimum sensitivity (left; top) and the corresponding mean gain (left; bottom) versus avalanche width for a 10Gb/s system using InAlAs (closed symbols) and InP (open symbols) APDs. Effective ionization coefficient ratio (right; top), gain-bandwidth product (right; middle), and tunnelling current density (right; bottom), as functions of avalanche width for a 10 Gb/s transmission system using InAlAs and InP. Lines are present to aid visualization.

8. Conclusions

In this chapter the impact ionisation process, from the perspective of APD detector design, has been introduced. The beneficial multiplicative effect on current, and the associated detrimental current fluctuations, excess noise, has been derived. The RPL model has been introduced. This model is routinely used to compute the multiplication and excess noise of thick and thin APD structures. A comprehensive survey of the measurement systems used to characterise the excess noise properties of photodiode structures has been presented, and two improved measurement systems have been suggested. A BER model which includes ISI, excess noise, and tunnelling current has been outlined. The key performance-determining factors which influence the APD and receiver design choices have been analysed. A comparison of InAlAs and InP APDs has been presented and InAlAs offers a marginal sensitivity improvement. An example 10 Gb/s detector and receiver combination has been presented for InAlAs and InP APDs.

9. Acknowledgements

The work reported here was carried out in the Department of Electronic and Electrical Engineering at the University of Sheffield, UK, within the research group of Prof. John David and Dr. Jo Shien Ng, whom the authors thank most sincerely for securing the necessary funding and helping to direct the work.

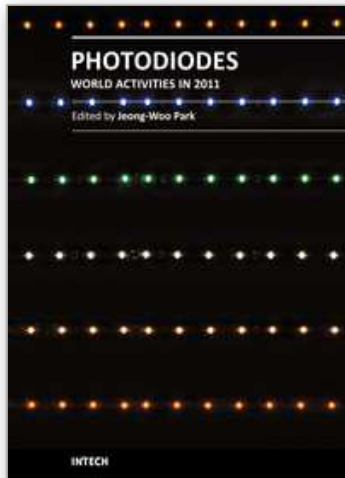
Daniel S. G. Ong is funded by the University of Sheffield studentship and James E. Green is funded by Engineering and Physical Sciences Research Council (EPSRC).

10. References

- Agrawal, G. P. (1997). *Fiber-Optic Communication Systems*, 2nd ed New York, John Wiley & Sons, Inc.
- Ando, H. & Kanbe, H. (1981). Ionization coefficient measurement in GaAs by using multiplication noise characteristics. *Solid-State Electronics*, 24, 629-634.
- Baertsch, R. D. (1966). Low-frequency noise measurements in silicon avalanche photodiodes. *IEEE Transactions on Electron Devices*, ED13, 383-385.
- Bulman, G. E. (1983). *The experimental determination of impact ionisation coefficients in GaAs and InP*. PhD thesis, University of Illinois.
- Campbell, J. C. (2007). Recent advances in telecommunications avalanche photodiodes. *Journal of Lightwave Technology*, 25, 109-121.
- Forrest, S. R., DiDomenico, M., Jr., Smith, R. G. & Stocker, H. J. (1980a). Evidence for tunneling in reverse-biased III-V photodetector diodes. *Applied Physics Letters*, 36, 580-582.
- Forrest, S. R., Leheny, R. F., Nahory, R. E. & Pollack, M. A. (1980b). In_{0.53}Ga_{0.47}As photodiodes with dark current limited by generation-recombination and tunneling. *Applied Physics Letters*, 37, 322-325.
- Goh, Y. L., Marshall, A. R. J., Massey, D. J., Ng, J. S., Tan, C. H., Hopkinson, M., David, J. P. R., Jones, S. K., Button, C. C. & Pinches, S. M. (2007a). Excess avalanche noise in In_{0.52}Al_{0.48}As. *IEEE Journal of Quantum Electronics*, 43, 503-507.
- Goh, Y. L., Massey, D. J., Marshall, A. R. J., Ng, J. S., Tan, C. H., Ng, W. K., Rees, G. J., Hopkinson, M., David, J. P. R. & Jones, S. K. (2007b). Avalanche multiplication in InAlAs. *IEEE Transactions on Electron Devices*, 54, 11-16.
- Kinsey, G. S., Hansing, C. C., Holmes, A. L., Streetman, B. G., Campbell, J. C. & Dentai, A. G. (2000). Waveguide In_{0.53}Ga_{0.47}As-In_{0.52}Al_{0.48}As avalanche photodiode. *IEEE Photonics Technology Letters*, 12, 416-418.
- Lau, K. S., Tan, C. H., Ng, B. K., Li, K. F., Tozer, R. C., David, J. P. R. & Rees, G. J. (2006). Excess noise measurement in avalanche photodiodes using a transimpedance amplifier front-end. *Measurement Science & Technology*, 17, 1941-1946.
- Li, K. F. (1999). *Avalanche noise in submicron GaAs and InP structures*. PhD thesis, University of Sheffield.
- Li, K. F., Ong, D. S., David, J. P. R., Rees, G. J., Tozer, R. C., Robson, P. N. & Grey, R. (1998). Avalanche multiplication noise characteristics in thin GaAs p⁺-i-n⁺ diodes. *IEEE Transactions on Electron Devices*, 45, 2102-2107.
- Marshall, A. R. J., Goh, Y. L., Tan, L. J. J., Tan, C. H., Ng, J. S. & David, J. P. R. (2006). A comparison of the lower limit of multiplication noise in InP and InAlAs based APDs for telecommunications receiver applications. *2006 IEEE LEOS Annual Meeting Conference Proceedings, Vols 1 and 2*, 789-790.

- McIntyre, R. J. (1966). Multiplication noise in uniform avalanche diodes. *IEEE Transactions on Electron Devices*, ED13, 164-168.
- Ong, D. S., Li, K. F., Rees, G. J., David, J. P. R. & Robson, P. N. (1998). A simple model to determine multiplication and noise in avalanche photodiodes. *Journal of Applied Physics*, 83, 3426-3428.
- Ong, D. S. G., Ng, J. S., Hayat, M. M., Sun, P. & David, J. P. R. (2009). Optimization of InP APDs for high-speed lightwave systems. *Journal of Lightwave Technology*, 27, 3294-3302.
- Singh, J. (1995). *Semiconductor Optoelectronics: Physics and Technology*, McGraw-Hill.
- Stillman, G. E. & Wolfe, C. M. (1977). Avalanche photodiodes. In: *Semiconductors and semimetals*, R. K. Williardson & A. C. Beer (eds.), 291-393. Academic Press, Inc.
- Sun, P., Hayat, M. M., Saleh, B. E. A. & Teich, M. C. (2006). Statistical correlation of gain and buildup time in APDs and its effects on receiver performance. *Journal of Lightwave Technology*, 24, 755-768.
- Tager, A. S. (1965). Current fluctuations in a semiconductor (dielectric) under the conditions of impact ionization and avalanche breakdown. *Soviet Physics Solid State*, 6, 1919-1925.
- Tan, L. J. J., Ng, J. S., Tan, C. H. & David, J. P. R. (2008). Avalanche noise characteristics in submicron InP diodes. *IEEE Journal of Quantum Electronics*, 44, 378-382.
- Tan, L. J. J., Ong, D. S. G., Ng, J. S., Tan, C. H., Jones, S. K., Qian, Y. H. & David, J. P. R. (2010). Temperature dependence of avalanche breakdown in InP and InAlAs. *IEEE Journal of Quantum Electronics*, 46, 1153-1157.
- Toivonen, M., Salokatve, A., Hovinen, M. & Pessa, M. (1992). GaAs/AlGaAs delta-doped staircase avalanche photodiode with separated absorption layer. *Electronics Letters*, 28, 32-34.
- Wei, J., Dries, J. C., Wang, H. S., Lange, M. L., Olsen, G. H. & Forrest, S. R. (2002). Optimization of 10-Gb/s long-wavelength floating guard ring InGaAs-InP avalanche photodiodes. *IEEE Photonics Technology Letters*, 14, 977-979.
- Xie, F. Z., Kuhl, D., Bottcher, E. H., Ren, S. Y. & Bimberg, D. (1993). Wide band frequency response measurements of photodetectors using low-level photocurrent noise detection. *Journal of Applied Physics*, 73, 8641-8646.

IntechOpen



Photodiodes - World Activities in 2011

Edited by Prof. Jeong Woo Park

ISBN 978-953-307-530-3

Hard cover, 400 pages

Publisher InTech

Published online 29, July, 2011

Published in print edition July, 2011

Photodiodes or photodetectors are in one boat with our human race. Efforts of people in related fields are contained in this book. This book would be valuable to those who want to obtain knowledge and inspiration in the related area.

How to reference

In order to correctly reference this scholarly work, feel free to copy and paste the following:

Daniel S. G. Ong and James E. Green (2011). Avalanche Photodiodes in High-Speed Receiver Systems, Photodiodes - World Activities in 2011, Prof. Jeong Woo Park (Ed.), ISBN: 978-953-307-530-3, InTech, Available from: <http://www.intechopen.com/books/photodiodes-world-activities-in-2011/avalanche-photodiodes-in-high-speed-receiver-systems>

INTECH
open science | open minds

InTech Europe

University Campus STeP Ri
Slavka Krautzeka 83/A
51000 Rijeka, Croatia
Phone: +385 (51) 770 447
Fax: +385 (51) 686 166
www.intechopen.com

InTech China

Unit 405, Office Block, Hotel Equatorial Shanghai
No.65, Yan An Road (West), Shanghai, 200040, China
中国上海市延安西路65号上海国际贵都大饭店办公楼405单元
Phone: +86-21-62489820
Fax: +86-21-62489821

© 2011 The Author(s). Licensee IntechOpen. This chapter is distributed under the terms of the [Creative Commons Attribution-NonCommercial-ShareAlike-3.0 License](#), which permits use, distribution and reproduction for non-commercial purposes, provided the original is properly cited and derivative works building on this content are distributed under the same license.

IntechOpen

IntechOpen